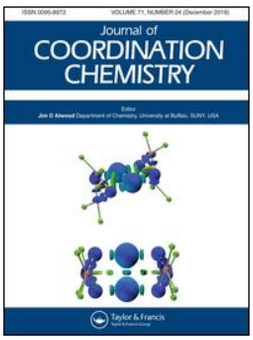

Journal of Coordination Chemistry

ISSN: 0095-8972 (Print) 1029-0389 (Online) Journal homepage: https://www.tandfonline.com/loi/gcoo20

Structurally different domains embedded half-sandwich arene Ru(II) complex: DNA/HSA binding and cytotoxic studies

V. O. Yadhukrishnan, Mathiyan Muralisankar, Ramachandran Dheepika, Ramaiah Konakanchi, Nattamai S. P. Bhuvanesh & Samuthira Nagarajan

To cite this article: V. O. Yadhukrishnan, Mathiyan Muralisankar, Ramachandran Dheepika, Ramaiah Konakanchi, Nattamai S. P. Bhuvanesh & Samuthira Nagarajan (2020): Structurally different domains embedded half-sandwich arene Ru(II) complex: DNA/HSA binding and cytotoxic studies, Journal of Coordination Chemistry, DOI: 10.1080/00958972.2020.1782895

To link to this article: https://doi.org/10.1080/00958972.2020.1782895

JOURNAL OF COORDINATION CHEMISTRY
https://doi.org/10.1080/00958972.2020.1782895

Structurally different domains embedded half-sandwich arene Ru(II) complex: DNA/HSA binding and cytotoxic studies

V. O. Yadhukrishnan[a], Mathiyan Muralisankar[a], Ramachandran Dheepika[a], Ramaiah Konakanchi[b], Nattamai S. P. Bhuvanesh[c] and Samuthira Nagarajan[a]

[a]Department of Chemistry, Central University of Tamil Nadu, Thiruvarur, Tamilnadu, India;
[b]Department of Chemistry, National Institute of Technology, Warangal, Telangana, India;
[c]Department of Chemistry, Texas A & M University, College Station, TX, USA

ABSTRACT

In this investigation, we have designed and synthesized a new Ru(II)-arene complex with triarylamine thiosemicarbazone hybrid ligand to explore its cytotoxicity. The ligand and the complex were well characterized by spectroscopic techniques. From the single-crystal X-ray crystallography, the molecular structure of the ligand was confirmed to be monoclinic lattice with *C12/C1* space group symmetry. X-ray photoelectron spectroscopy(XPS) studies ensured that ruthenium is in +2 oxidation state. The synthesized Ru(II)-arene complex was thoroughly investigated for the *in vitro* activity against human breast carcinoma (MCF-7), human colon carcinoma (COLO 205), human neuroblastoma (IMR-32), murine microphage (Raw 264.7) and embryonic kidney (HEK 293) using MTT assay. The interaction of the Ru(II)-arene complex with DNA/protein was also explored by absorption and emission spectral methods. This investigation highlights the role of hybrid ligand and its Ru(II) complex toward high cytotoxicity *in vitro*. The complex has high cytotoxic effect with IC_{50} value of $5.18 \pm 1.128\,\mu M$ toward human breast carcinoma cell line.

ARTICLE HISTORY
Received 9 April 2020
Accepted 9 June 2020

KEYWORDS
Triarylamine; thiosemicarbazone; arene Ru(II) complex: DNA binding; cytotoxicity

CONTACT Samuthira Nagarajan snagarajan@cutn.ac.in Department of Chemistry, Central University of Tamil Nadu, Thiruvarur 610005, India

Supplemental data for this article can be accessed here.

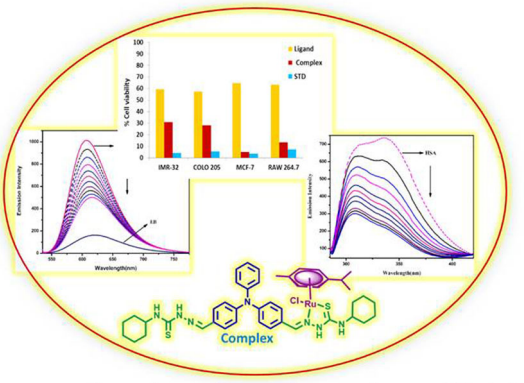

Ru(II)-arene complex with triarylamine-thiosemicarbazone hybrid ligands was designed, synthesised and investigated for the *in vitro* cytotoxicity studies. The complex possess good binding with DNA and HSA protein. The cytotoxicity study reveals that the complex is highly active against human breast carcinoma cell line (MCF-7).

1. Introduction

Metallo-anticancer drug development is an important and dynamic area of research which drives the bioinorganic pharmaceutical findings toward life-changing inventions [1–5]. Platinum-based drugs such as cisplatin, carboplatin, oxaliplatin, etc. have been the benchmark agents to treat many types of cancers in the human body, but their toxicity levels are relatively higher [6–9]. Developing new chemotherapeutics for treating platinum-resistant tumors with less toxicity and higher activity has gained global attraction. The journey to find alternative anticancer metal-based drugs other than platinum compounds is a very interesting research around the Globe. The ligand exchange kinetics of ruthenium complexes is comparable with platinum(II) complexes; the ligand exchange processes are quite slow and may take hours (rates 10^{-3} to 10^{-2} s^{-1}) [10–15].

Among the ruthenium complexes investigated, Ru(II)-arene half-sandwich complexes with a piano stool geometry have gained increased attention due to their diverse activity with respect to the chelating ligands [16–19]. Sadler's and coworkers [20–22] complexes (N,N-chelating ligands) bind specifically to N7 of guanine and exhibited high cytotoxicity against human ovarian cancer cell line (A2780). Likewise, Ru(II)-arene complexes with various ligands such as quinoxalinone [23], phenanthroline [24] and carboline [25] have been successfully investigated for their antitumor activity. Recently, the study of thiosemicarbazone (TSC) is gaining attention due to its success in clinical trials. Traynor *et al*. [26] and Stacy *et al.* [27] have reported on 3-aminopyridine-2-carboxaldehyde TSCs and their clinical trials (II Phase) for antineoplastic activity. Prophylaxis against both vaccinia and smallpox viruses [28] by methisazone have been reported by Hall *et al.* [29]. Among the various complexes studied imidazolium Ru(III) complexes are in phase II trials. To be specific, in 2017, KP1019 has a new formulation

to resolve the solubility issue and named as NKP-1339, approved by the FDA. In addition, it is very important to note that the former formulations are abandoned.

The combination of TSC ligands with many other biologically significant compounds as co-ligands has been used in various applications [30–32]. Triarylamines (TAA) are being studied for multiple applications, including electronic, bioinorganic, etc.; they are easily soluble and highly fluorescent. Owing to these properties they have been successfully administrated as probes and markers for DNA [33, 34]. They possess a unique style of interaction with DNA and can exclusively bind to quadruplex DNA [35, 36]. Chennoufi *et al.* [37] have investigated on water-soluble pyridine substituted triphenylamine target cytosolic organelles of living cells by apoptosis induced by two photon absorption. They stated that photoactivation is related to mitochondrial apoptotic pathway by reactive oxygen species (ROS) production.

In this work, in order to improve the activity of ruthenium(II)-arene complexes, we have designed ligand with biologically active TSC and TAA. Hybrid architecture of ligand is acknowledged as sterically flexible owing to its intramolecular hydrogen bonding and co-ligand effect over the azomethine carbon atom. In addition, π-π stacking interactions also help to improve the binding [38, 39]. The interaction of complex with DNA and human serum albumin (HSA) was studied by spectroscopic methods. The *in vitro* activity of these complexes is examined by MTT assay, antiproliferative assay using human breast carcinoma cell line (MCF-7), human colon carcinoma cell line (COLO 205), human neuroblastoma cell line (IMR-32) and murine microphage cell lines (Raw 264.7). This investigation will give valuable idea about the role of hybrid ligand and its cytotoxic activity to the organometallic research community.

2. Experimental

2.1. Materials and methods

All reagents were purchased from Sigma Aldrich (Bangalore, India) and used as received. The melting point of the synthesized complex was measured by Lab India instrument and produced as uncorrected. Electronic absorption spectra were taken in the range 200–800 nm using a Jasco spectrophotometer. FT- IR spectra in the range of 4000–500 cm^{-1} were obtained using a Perkin-Elmer Frontier FT-IR spectrophotometer. Jasco V-630 was used for obtaining the emission spectra in dimethyl formamide (DMF). Both ^{1}H and ^{13}C NMR spectra were recorded in $CDCl_3$ solvent with Tetramethylsilane (TMS) as an internal standard using a Bruker spectrometer (400 and 100 MHz, respectively). Electron spray ionization-mass spectrometry (ESI-MS) analysis of ligand and complex were recorded on a Thermo ExactivePlus mass spectrometer.

2.2. Synthesis

2.2.1. Synthesis procedure of ligand

Triarylamine (TAA) aldehyde was added to a methanolic solution of 4-cyclohexyl thiosemicarbazide with a few drops of glacial acetic acid, and the resulting mixture was heated at 60–70 °C for 6 h. The solution was cooled to room temperature to afford a

yellow solid, and was filtered, washed with ethanol, and dried in *vacuum*. Methanol and acetonitrile (1:1) mixture was allowed to evaporate slowly to get suitable crystals of compound for XRD analysis. Yield: 86%. Yellow solid. M.p. 236 °C. ESI- MS (*m/z*) Calcd. for $C_{34}H_{41}N_7S_2$ $[M+H]^+$ 612.2943, found 612.2855. Anal. Calc. for $C_{34}H_{41}N_7S_2$: C, 66.74; H, 6.75; N, 16.02; S, 10.48. Found: C, 66.91; H, 6.73; N, 16.01; S, 10.43. UV–vis (DMF), λ_{max} (nm): 213, 386. FT-IR (ATR, cm^{-1}): ν(N-H); 3328(m), ν(C-H); 2930(s), ν(C = N); 1589(s), ν(C = S); 1267(s). ^{1}H NMR (400 MHz, $CDCl_3$), δ(ppm): 10.23 (s, 2H, =N-NH), 7.90 (s, 2H, HC = N), 7.52 (d, $J = 8.0$ Hz, 4H), 7.32 (d, $J = 6.8$ Hz, 3H), 7.14 (d, $J = 8.0$ Hz, 2H), 7.08 (d, $J = 8.4$ Hz, 4H), 4.31–4.24 (m, 2H), 2.09 (s, 2H, cyclohexyl-NH)) 1.76–1.63 (m, 8H), 1.46–1.39 (m, 4H), 1.34–1.21 (m, 8H). ^{13}C NMR (100 MHz, $CDCl_3$), δ(ppm): 175.44 (C = S), 146.32 (C = N), 129, 128, 127, 125, 124, 123 (aromatic carbons), 52.83, 32.77, 25.50, 24.75 (aliphatic carbons).

2.2.2. Synthesis of [(η^6-p-cymene)-Ru^{II}(ligand)Cl]Cl

[(η^6-*p*-cymene)-Ru^{II}(Cl)$_2$]$_2$ was synthesized as per the reported method [40]. The prepared Ru(II)-(η^6-*p*- cymene) dimer (0.100 g, 0.2 mmol) and ligand were combined in 20 mL of CH_2Cl_2 and the resultant mixture was stirred for 12–14 h at room temperature. The color of the reaction mixture changed to dark red. The dark red solution was concentrated under reduced pressure, and the addition of hexane (20 mL) gave an orange solid. The product was collected by filtration, washed with hexane, and dried in *vacuum*. Yield: 78%. Orange solid. M.p: 216 °C. ESI- MS (*m/z*) Calcd. for $C_{44}H_{56}Cl_2N_7RuS_2$ $[M\text{-}2Cl\text{-}H]^+$ 846.2926, found 846.2816. UV–vis (DMF), λ_{max} (nm): 214, 398, 540. Anal. Calc. for $C_{44}H_{55}N_7RuS_2$: C, 59.88; H, 6.28; N, 11.11; S, 7.21. Found: C, 60.02; H, 6.27; N, 11.08; S, 7.29. FT-IR (ATR, cm^{-1}): ν(N-H); 3347(m), ν(C-H); 2968(s), ν(C = N); 1580(s), ν(C = S); 1241(s). ^{1}H NMR (400 MHz, $CDCl_3$), δ(ppm): 14.42 (s, 1H, $=N-NH$), 8.73 (s, 1H, HC = N), 8.08 (d, $J = 8.4$ Hz, 1H), 7.37 (t, $J = 8.0$ Hz, 4H), 7.20 (d, $J = 7.2$ Hz, 6H), 7.14 (d, $J = 8.4$ Hz, 1H), 7.08 (d, $J = 8.4$ Hz, 2H), 5.49 (d, $J = 6.0$ Hz, 1H, p-cym-H), 5.10 (d, $J = 6.0$ Hz, 1H, *p*-cym-H), 5.01 (d, $J = 5.2$ Hz, 1H) 4.97 (d, $J = 1.6$ Hz, 1H, *p*-cym-H), 2.72–2.66 (m, 2H, p-cym $CH(CH_3)_2$), 2.12 (s, 3H, *p*-cym (CH_3)), 2.02 (s, cyclohexane attached N − 3H) 1.20 (d, $J = 6.8$ Hz, 3H, *p*-cym $C(CH_3)_2$), 1.14 (d, $J = 6.8$ Hz, 3H, *p*-cym $C(CH_3)_2$), 1.77–1.61 (m, 4H), 1.61–1.57 (m, 8H), 1.50–1.46 (m, 2H), 1.44–1.35 (m, 8H). ^{13}C NMR (100 MHz, $CDCl_3$), δ(ppm): 175.59 (C = S), 148.82(C = N), 132, 129, 128, 125, 124, 123 (aromatic carbons), 103.50, 88.55, 87.94, 82.66 (carbons of *p*-cymene), 52.87, 32.76, 30.71, 25.51, 24.76, 21.40, 18.56 (aliphatic carbons).

2.3. DNA-binding studies

DNA is recognized as the primary target of many metal-based anticancer drugs. Most of the metal complexes exert their effects through binding with DNA, which is the critical step to evaluate the effectiveness of metal-based drugs. As a result, the elucidation of non-covalent interactions between DNA and complex was investigated with the help of different techniques. The UV–vis absorption spectroscopic studies for DNA-binding analysis were performed at room temperature. CT-DNA sample was dissolved in 50 mM NaCl/5 mM TrisHCl (pH 7.2) solution. The CT-DNA solution (without complex) showed an absorbance at 260 nm with 6600 M^{-1} cm^{-1} extinction coefficient, indicating

that the CT-DNA was in protein-free form [41]. Stock solutions were stored at 4 °C and used within 4 days. About 0–50 μM of CT-DNA was added to the fixed concentration of complex. The spectra were recorded after equilibration for three min, allowing the compounds to bind with CT-DNA. Complex of required concentration was prepared by dissolving the calculated amount of complex in 5% DMF/TrisHCl/NaCl.

The competitive binding of each complex with EB was investigated by fluorescence spectroscopic techniques, thus examining whether the complex can displace EB from its CT-DNA-EB complex. EB solution was prepared using TrisHCl/NaCl buffer (pH 7.2). The test solution was added in aliquots of 2.5 μM concentration to DNA-EB and the change in fluorescence intensities at 596 nm (excitation at 450 nm) was recorded.

2.4. HSA-binding studies

The fluorescence emission spectroscopy was utilized to study the binding of Ru(II)-arene complex with HSA. The experiments were carried out at a fixed excitation wavelength (corresponding to HSA) at 280 nm and monitoring the emission at 335 nm. Stock solution of HSA was prepared in Tris-buffer (50 mM NaCl/5 mM Tris-HCl, pH 7.2) and stored in the dark at 4 °C. HSA (2.5 mL) solution was titrated by consecutive additions of 10^{-6} M of complex. The synchronous fluorescence spectra measurements were obtained at the same concentration of HSA and the complex. The spectra were measured at two different $\Delta\lambda$ (difference between the excitation and emission wavelengths of HSA) values of 15 and 60 nm.

2.5. Antiproliferative activity and MTT assay

The human breast carcinoma cell line (MCF-7), human colon carcinoma cell line (COLO 205), human neuroblastoma cell line (IMR-32) and murine microphage cell line (Raw 264.7) were obtained from National Centre for Cell Science (NCCS), Pune and grown in Dulbecco's Modified Eagles Minimum (DMEM) containing 10% fetal bovine serum (FBS), amphotericin (3 μg mL^{-1}), gentamycin (400 μg mL^{-1}), streptomycin (250 μg mL^{-1}) and penicillin (250 units mL^{-1}) in a carbon dioxide incubator at 5% CO_2. About 700 cells/well were seeded in a 96-well plate using culture medium, the viability was tested using trypan blue dye with the help of a haemocytometer and 95% of viability was confirmed. After 24 h, the new medium with compounds in the concentration of 100, 10 and 1 μg mL^{-1} were added at respective wells and kept at incubation for 48 h. After incubation MTT assay was performed [42].

After 48 h of drug treatment, the medium was changed again for all groups and 10 μL of MTT (5 mg mL^{-1} stock solution) was added and the plates were incubated for an additional 4 h. The medium was discarded and the formazan blue, which was formed in the cells, was dissolved with 50 μL of DMSO. The optical density was measured on a micro plate spectrophotometer at a wavelength of 570 nm. The percentage of cell inhibition was calculated using the following formula [43]:

$$\% \text{ Growth inhibition } = 100 - (A_i/A_o) \times 100$$

where A_i is the absorbance of the sample and A_o is the absorbance of the control.

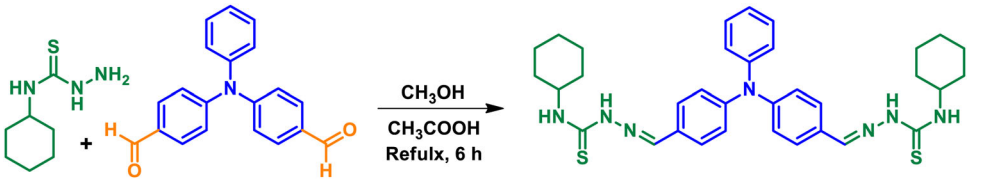

Scheme 1. Synthesis of ligand.

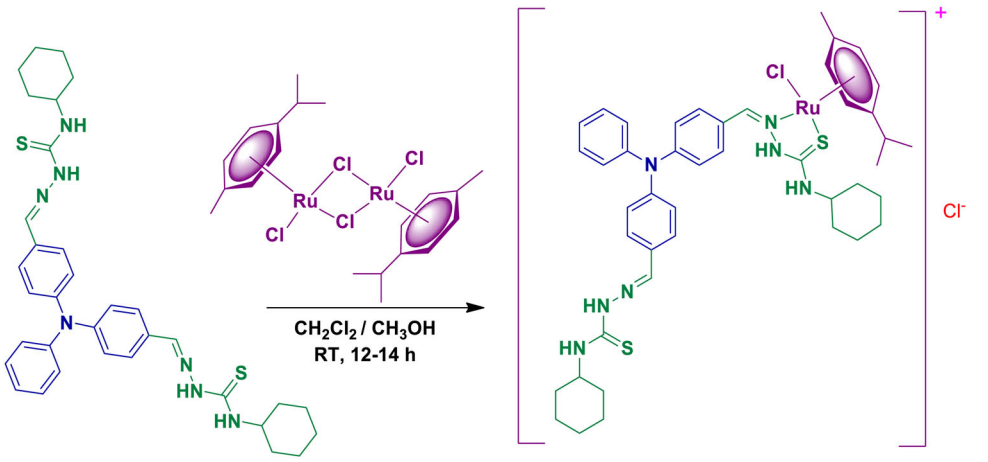

Scheme 2. Synthesis of complex.

Non-linear regression graph was plotted between % cell inhibition and Log_{10} concentration and IC_{50} was determined using Graph Pad Prism software.

3. Results and discussion

The hybrid ligand was synthesized through condensation reaction between 4-cyclohexyl thiosemicarbazide and triarylamine dialdehyde as shown in Scheme 1.

Ruthenium(II)(η^6-*p*-cymene) complex of the type [RuCl(η^6-*p*-cymene)ligand]Cl was synthesized by the reaction between [RuCl(μ-Cl)(η^6-*p*-cymene)]$_2$ and triarylamine-based TSC ligand (Scheme 2). Synthesized ligand and complex were characterized using UV–vis, FT-IR, NMR spectroscopic and mass spectrometric studies. The structure of the ligand was determined by single-crystal X-ray diffraction study.

3.1. Spectroscopy and crystal structure

The absorption spectrum of the ligand in DMF exhibited two characteristic bands (supporting information Figure S1). The bands at 213 and 318 are assigned to π-π^* and n-π^* transitions, respectively [44]. The complex also exhibited two prominent bands at 214 and 286 nm which correspond to π-π^* and n-π^* transitions, respectively (supporting information Figure S2). The additional bands at 392 and 540 nm were assigned to MLCT and d-d transitions [45]. Absorption spectra of the complex were taken in DMF

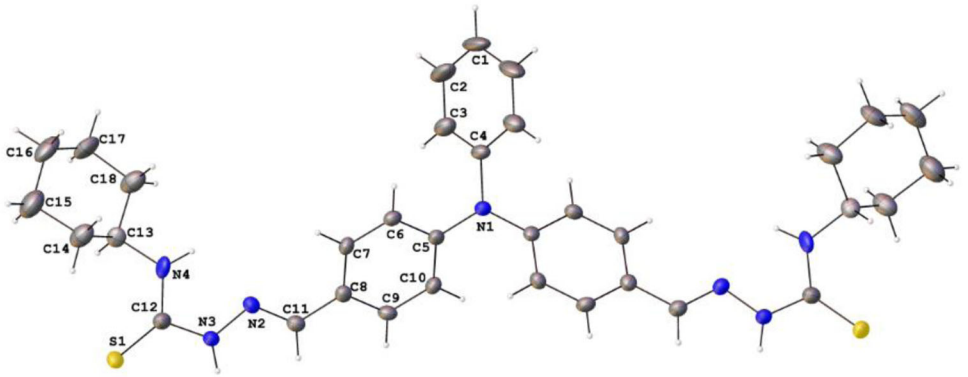

Figure 1. Thermal ellipsoid (50%) plot of ligand with atomic labeling.

for fresh solution and after five days. There were no changes observed in the spectra, which shows that ruthenium(II) complex is stable in the test solution [46]. FT-IR data of the TSC ligands show a characteristic peak at 3453 cm^{-1} due to ν(N – H). Other characteristic peaks are obtained at 1582 cm^{-1} and 1321 cm^{-1} which correspond to ν(C = N) and ν(C = S), respectively. After the complex formation, the stretching frequency of thiocarbonyl ν(C = S) decreases, indicating that the sulfur is coordinated with ruthenium ion [47].

^{1}H NMR spectrum of ligand exhibits (=N-NH) and azomethine (HC = N) protons were at 10.26 and 7.90 ppm (supporting information Figure S8). The same protons in the complex were deshielded and appeared at 14.56 ppm. The aromatic protons of the complex resonate in the range of 7.37–7.08 ppm. The new signals observed in the region 5.50–4.97 ppm are due to occurrence of *p*-cymene complex [48]. The signal due to cyclohexyl protons in the ligand and complex were displayed in the range of 4.30–3.89 ppm and 2.04–1.23 ppm (supporting information Figure S10). In the ^{13}C spectrum of ligand, thiocarbonyl (C = S) and imine (C = N) carbon signals appeared at 175.99 ppm and 146.32 ppm (supporting information Figure S9). All aromatic carbons in the ligand and complex appeared in the range of 149.61–119.74 ppm and 150.69–119.23 ppm. ^{13}C NMR spectrum of the complex, new signals at 103.95–82.12 ppm confirmed the presence of *p*-cymene group in complex (supporting information Figure S11).

The single-crystal XRD of the ligand shows the monoclinic lattice with *C12/C1* space group symmetry. The experimental details, crystallographic refinement parameters and selected bond lengths and angles are presented in supporting information Tables S1 and S2. Thermal ellipsoid plot of ligand with the atomic labeling scheme is shown in Figure 1. The ligand is typically composed of three different domains: TAA group connected to cyclohexyl by TSC moiety. The structure reveals that the central nitrogen atom of triarylamine is in sp^2 hybridization and the three phenyl rings are slightly tilted from the plane of the ring, existing in a propeller-like fashion [14]. The molecule has *E*-conformation with respect to the N2 – N3, the bond length is 1.370, 1.385, 1.380 and 1.386 Å and dihedral angle is 177.0°, 164.7°, 173.3° and 173.2° for ligand.

ESI-MS spectra of ligand and complex are shown in supporting information Figures S12 and S13, respectively, in positive scan mode. The spectrum of ligand shows

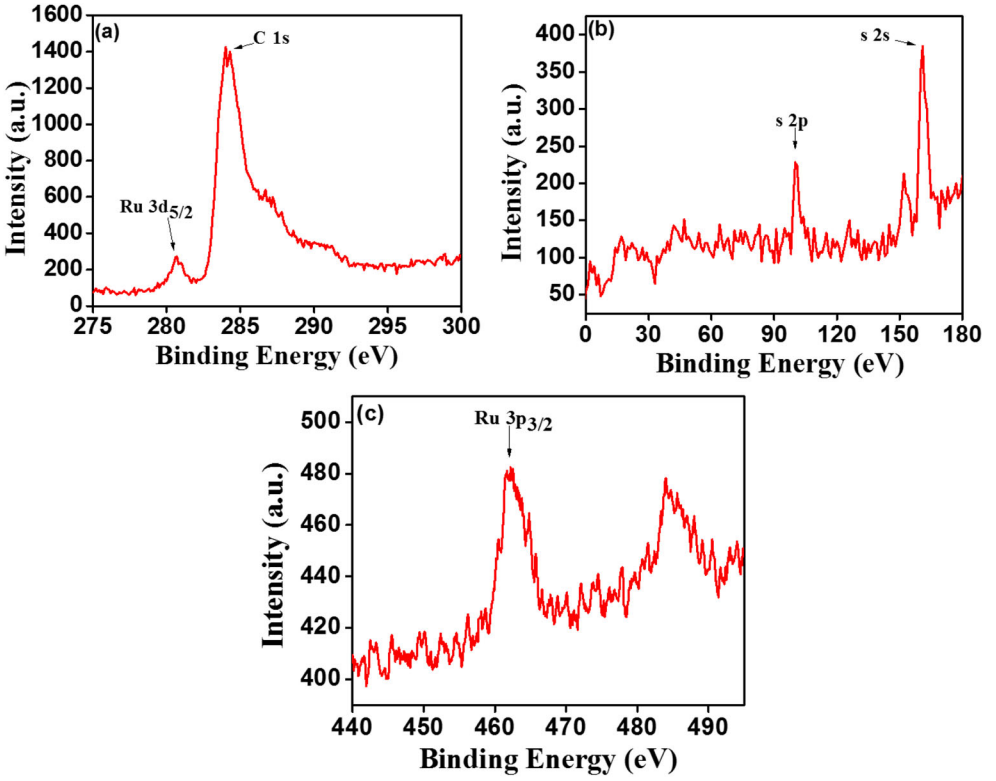

Figure 2. The narrow scan XPS spectra of complex.

$[M+H]^+$ peak as the base peak at 612.2865 *m/z*. Molecular ion peak for the complex was not observed due to possible fragmentation. The complex exhibits base peak at 846.2816 *m/z* due to $[M-2Cl\text{-}H]^+$, suggesting that the chloro ($2Cl^-$) group is labile [49].

The narrow scan XPS spectra of the elements Ru 3d, Ru 3p, C 1 s, S 2p and S 2 s are given in Figure 2. The presence of Ru $3d_{5/2}$ (280.64 eV) and Ru $3p_{3/2}$ (462 eV) peaks confirms that the ruthenium is present in the complex as Ru(II). S 2p (100 eV) and S 2 s (160 eV) suggest the formation of ruthenium-sulfur bond [50] and 1 s peak was obtained at 284.15 eV.

3.2. DNA interaction studies

3.2.1. Uv–visible titration

The electronic spectra of complex with and without CT-DNA are given in Figure 3. The changes observed in the electronic spectra accounts for the complex–CT–DNA interaction. From the spectra, it is found that the complex upon addition of CT-DNA exhibits hypochromism with 2-3 nm red-shift which can be indicative of intercalation mode of binding [51, 52]. The equilibrium constant (K_b) was found from the linear plot obtained using the equation:

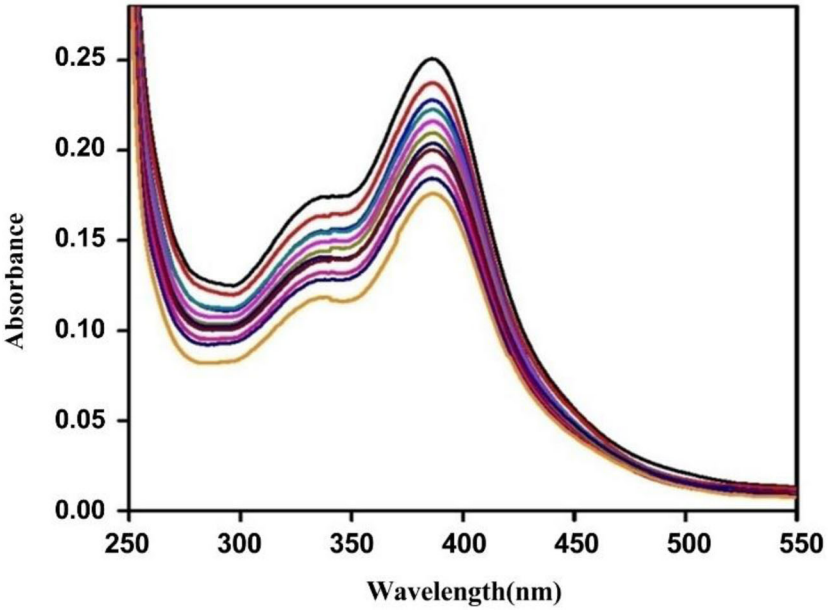

Figure 3. Absorption spectra of complex with CT-DNA in Tris-HCl buffer upon addition of CT-DNA. [Complex] = 1.5×10^{-5} M, [DNA] = 0 − 50 μM.

$$\frac{[\mathrm{DNA}]}{(\varepsilon_a - \varepsilon_f)} = [\mathrm{DNA}]/(\varepsilon_b - \varepsilon_f) + 1/K_b(\varepsilon_b - \varepsilon_f)$$

where [DNA] is the concentration on DNA in base pairs, ε_a is the apparent extinction coefficient calculated as $A_{(\mathrm{observed})}$/[complex], ε_f is the extinction coefficient for the free complex and ε_b is the extinction coefficient for the complex in the completely bound form. K_b was calculated from the plot of [DNA]/(ε_a-ε_f) *versus* [DNA] by taking the ratio of slope and intercept given in supporting information Figure S3. The binding constant was found to be 3.2×10^4 M^{-1}. The K_b found is matching with already reported similar complexes [53].

3.2.2. EB displacement studies

The prepared complex does not possess fluorescence in solution with CT-DNA at room temperature, thus the binding of complex with CT-DNA cannot be studied directly. The quenching of fluorescence of ethidium bromide (EB) bound to CT-DNA with the addition of complex is investigated. A decrease in the fluorescence is observed when the complex replaces EB from the CT-DNA and it gives an indirect evidence for the DNA binding. Figure 4 shows the interaction of complex with CT-DNA treated with EB. The fluorescence decreased upon each addition of the complex. The quenching of fluorescence confirms the displacement of EB from the CT-DNA by the ruthenium complex. The interactions obtained by fluorescence studies were quantitatively measured using the Stern-Volmer equation, $F^0/F = 1 + K_q[Q]$ [53], where F^0 and F are the fluorescence intensities in the presence and in the absence of the complex, K_q is the linear Stern-Volmer quenching constant and [Q] is the concentration of complex.

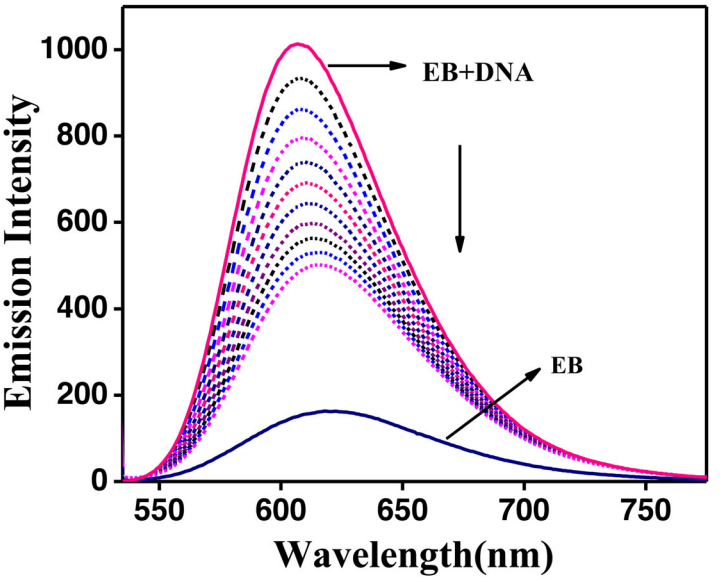

Figure 4. Fluorescence quenching curves of EB bound to DNA in the presence of complex. [DNA] = 5 μM, [EB] = 5 μM, and [complex] = 0 − 50 μM. Arrow shows decrease in emission upon increasing DNA concentration.

K_q is found from the slope of F^0/F *versus* [Q] and given in supporting information Figure S4.

The equation K_{EB}[EB]=K_{app}[complex] is used to calculate the apparent binding constant K_{app} [54], where [complex] is concentration of complex when the fluorescence intensity of EB is reduced to 50%. [EB] = 5 μM and $K_{EB} = 1.0 \times 10^7$. The results suggest that the complex binds with CT-DNA through intercalation mode interaction. K_q and K_{app} values were found to be 2.08×10^4 and 1.02×10^6 M^{-1}, respectively.

3.3. Protein-binding studies

3.3.1. Fluorescence spectroscopic studies

Emission spectra were obtained in a broad range of 290–450 nm on exciting at 280 nm. The fluorescence quenching of HSA upon adding the ruthenium complex was observed at 310 nm with 2–3 nm hypochromic shift. Changes in the spectra of complex are illustrated in Figure 5. The decrease in fluorescence intensity confirmed the interaction of complex with HSA. The shift in wavelength has proved that the interaction of complex and protein takes place at hydrophobic environment. Using the Stern-Volmer equation the quenching constant (K_q) was found to measure the interaction quantitatively from the plot of F^0/F *versus* [Q] (supporting information Figure S5). The Scatchard equation was used to find the equilibrium binding constant. Scatchard equation is given by $\log[(F^0\text{-}F)/F] = \log K_b + n\log[Q]$, where F^0 and F are the fluorescence in the absence and presence of the complex, K_b is the equilibrium binding constant and n is the number of binding sites [52]. The K_b is found from a plot of $\log[(F^0\text{-}F)/F]$ *versus* log [Q] (supporting information Figure S6). The ligand and complex showed binding constant values toward HSA of 1.18×10^5 and 9.78×10^5 M^{-1},

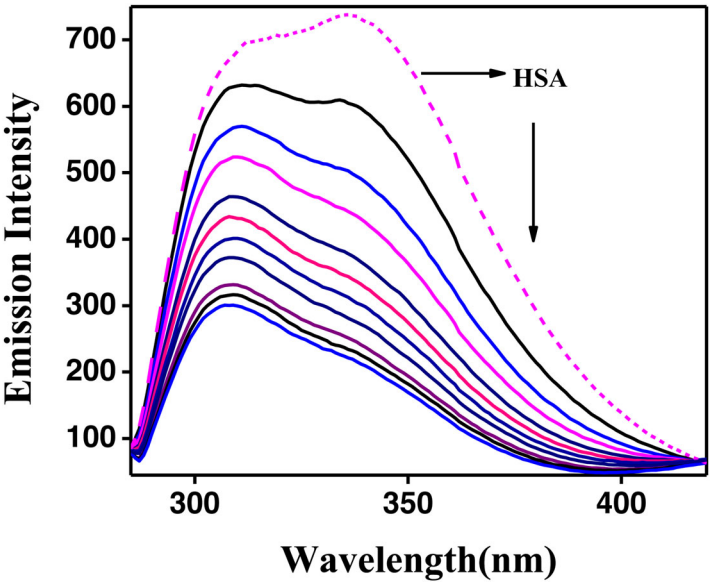

Figure 5. Fluorescence quenching curves of HSA in the absence and presence of complex. [HSA] = 1 μM and [complex] = 0–20 μM.

respectively. The values obtained from fluorescence data show that the complex has good binding affinity toward the HSA.

Beckford *et al.* [56] studied the biological behavior of a ruthenium-arene complex containing piperonal-based TSC ligands. The obtained binding constants for CT-DNA were in the range of 10^3 M^{-1}, where complex in this study shows better binding in the range of 10^4 M^{-1}. The combination of ligands with Ru metal has exhibited DNA and protein-binding constants which is comparable with our complex [54, 55]. Subasi *et al.* [57] reported a similar kind of study on ruthenium-arene complex with pyrrole ring containing TSC ligand gives binding constant in the range 10^4 M^{-1} toward CT-DNA. Similarly, in another report Muralisankar *et al.* [58] reported DNA- and protein-binding studies of TSC containing complexes are in the range of 10^4 M^{-1} and protein-binding constant in the range of 10^5 M^{-1}.

3.4. In vitro antiproliferative evaluation

The antiproliferative activity of the newly synthesized compounds was evaluated against different cancer cell lines such as IMR-32 (neuroblastoma), MCF-7 (breast), COLO 205 (colon), Raw 264.7 (murine) and HEK293 (embryonic kidney) by using the 3-(4,5-dimethylthiazol-2-yl)-2,5-diphenyltetrazolium bromide (MTT) method [53]. The MTT assay results were shown in IC_{50}, expressed in micromolar units and summarized in Table 1. The percentage of cell viability *versus* concentration graphs is shown in supporting information Figure S7. Cisplatin was used as a positive control. The results clearly indicate that the complex exhibited potent antiproliferative activity against MCF-7 and Raw 264.7 with IC_{50} values of 5.18 ± 1.128 μM [38] and 13.29 ± 1.0.21 μM [39], respectively, compared to standard drug cisplatin (IC_{50} = 3.78 ± 1.088 and 7.24 ± 0.156 μM). Similarly the complex showed good activity against IMR-32

Table 1. IC_{50} values of synthesized compounds against IMR-32, COLO 205, MCF-7, RAW 264.7 and HEK 293 cell lines.

	IC_{50} (μM)				
Comp.	IMR-32	COLO 205	MCF-7	Raw 264.7	HEK 293
Ligand	59.24 ± 1.068	57.42 ± 0.514	64.57 ± 1.893	63.23 ± 1.023	ND
Complex	30.88 ± 1.047	28.07 ± 1.342	5.18 ± 1.128	13.29 ± 1.021	38.72 ± 1.121
STD	4.29 ± 1.125	5.68 ± 1.057	3.78 ± 1.088	7.24 ± 0.156	ND

(30.88 ± 1.047 μM) [54] and COLO 205 (28.07 ± 1.342 μM) [41], respectively. In addition, we have also tested the toxicity of the complex against HEK293 normal cell line, the IC_{50} values of 38.72 ± 1.121 μM. Interestingly, the complex has superior cytotoxic effect with IC_{50} value of 5.18 ± 1.128 μM toward human breast carcinoma cell line (MCF-7) among the cell lines studied, which is comparable with the standard drug cisplatin and few similar molecules. Demoro *et al.* [59] have investigated binuclear TSC ruthenium complexes with nitrofuryl groups as potential antitumor agents, where the IC_{50} value was in the range of 8.7–30 μM against MCF-7. In another study, Anitha *et al.* [60] have shown that complexes with TSC/semicarbazone bearing 9,10-phenanthrenequinone groups exhibited IC_{50} from 13 to 39 μM. The complex has better cytotoxicity than the 9-anthraldehyde TSC substituted Ru complexes reported by Beckford *et al.* [56]. The impressive cytotoxicity of complex against MCF-7 cancer lines has proven them to be new promising candidate in anticancer research.

4. Conclusion

Triarylamine-TSC hybrid ligand and its Ru(II) complex as an anticancer agent has been synthesized and characterized by various techniques. The single-crystal X-ray diffraction study confirmed the structure of the ligand; the monoclinic lattice with *C12/C1* space group symmetry. XPS spectra evidently showed that ruthenium is present in the complex in +2 oxidation state. The interaction of complex with CT-DNA was calculated to be 3.2×10^4 M^{-1}. The complex showed 9.78×10^5 M^{-1} binding constant values, toward HSA. *In vitro* studies of the ligand and complex against five different cell lines, IMR-32, COLO 205, MCF-7, RAW 264.7 and HEK 293, are analyzed. The complex showed moderate activity against COLO 205, IMR-32 and HEK293. Interestingly, the complex has superior cytotoxic effect with IC_{50} value of 5.18 ± 1.128 μM toward human breast carcinoma cell line (MCF-7) among the cell lines studied, which is comparable with the standard drug cisplatin. On summation of the studies, the cytotoxicity role of hybrid combination of ligands and its Ru(II)-arene complex have been explained and they can be potentially used as ideal anticancer agents.

Disclosure statement

No potential conflict of interest was reported by the authors.

Acknowledgements

M.S. thanks the Department of Science and Technology and Ministry of Science and Technology, Government of India for Post-Doctoral Fellowship under SERB-NPDF program.

Funding

S.N. gratefully acknowledges DST-SERB for the financial support.

References

[1] C. Santini, M. Pellei, V. Gandin, M. Porchia, F. Tisato, C. Marzano. *Chem. Rev.*, **114**, 815 (2014).
[2] B. Englinger, C. Pirker, P. Heffeter, A. Terenzi, C.R. Kowol, B.K. Keppler, W. Berger. *Chem. Rev.*, **119**, 1519 (2019).
[3] I.R. Canelon, P.J. Sadler. *Inorg. Chem.*, **52**, 12276 (2013).
[4] A.L. Laine, C. Passirani. *Curr. Opin. Pharmacol.*, **12**, 420 (2012).
[5] M.J. Hannon. *Pure Appl. Chem.*, **79**, 2243 (2007).
[6] P. Jordan, M. Carmo-Fonseca. *Cell. Mol. Life Sci.*, **57**, 1229 (2000).
[7] H. Cui, R. Goddard, K.R. Porschke, A. Hamacher, M.U. Kassack. *Inorg. Chem.*, **55**, 2986 (2016).
[8] D. Pollak, R. Goddard, K.R. Porschke. *Inorg. Chem.*, **55**, 9424 (2016).
[9] D. Picone, F. Donnarumma, G. Ferraro, G. Gotte, A. Fagagnini, G. Butera, M. Donadelli, A. Merlino. *J. Inorg. Biochem.*, **173**, 105 (2017).
[10] J. Haribabu, G. Sabapathi, M.M. Tamizh, C. Balachandran, N.S.P. Bhuvanesh, P. Venuvanalingam, R. Karvembu. *Organometallics*, **37**, 1242 (2018).
[11] E.S. Antonarakis, A. Emadi. *Cancer Chemother. Pharmacol.*, **66**, 1 (2010).
[12] C.M. Clavel, E. Păunescu, P. Nowak-Sliwinska, A.W. Griffioen, R. Scopelliti, P.J. Dyson. *J. Med. Chem.*, **58**, 3356 (2015).
[13] I. Kostova. *Curr. Med. Chem.*, **13**, 1085 (2006).
[14] A. Bergamo, C. Gaiddon, J.H.M. Schellens, J.H. Beijnen, G.J. Sava. *J. Inorg. Biochem.*, **106**, 90 (2012).
[15] J. Reedijk. *Platin. Met. Rev.*, **52**, 2 (2008).
[16] L. Zeng, P. Gupta, Y. Chen, E. Wang, L. Ji, H. Chao, Z.-S. Chen. *Chem. Soc. Rev.*, **46**, 5771 (2017).
[17] A.A. Nazarov, C.G. Hartinger, P.J. Dyson. *J. Organomet. Chem.*, **751**, 251 (2014).
[18] K. Jeyalakshmi, J. Haribabu, C. Balachandran, S. Swaminathan, N.S.P. Bhuvanesh, R. Karvembu. *Organometallics*, **38**, 753 (2019).
[19] P. Li, W. Su, X. Lei, Q. Xiao, S. Huang. *Appl. Organomet. Chem.*, **31**, 3685 (2017).
[20] R.E. Morris, R.E. Aird, P. del, S. Murdoch, H. Chen, J. Cummings, N.D. Hughes, S. Parsons, A. Parkin, G. Boyd, D.I. Jodrell, P.J. Sadler. *J. Med. Chem.*, **44**, 3616 (2001).
[21] H. Chen, J.A. Parkinson, S. Parsons, R.A. Coxall, R.O. Gould, P.J. Sadler. *J. Am. Chem. Soc.*, **124**, 3064 (2002).
[22] H.K. Liu, P.J. Sadler. *Acc. Chem. Res.*, **44**, 349 (2011).
[23] W. Ginzinger, G. Muhlgassner, V.B. Arion, M.A. Jakupec, A. Roller, M. Galanski, M. Reithofer, W. Berger, B.K. Keppler. *J. Med. Chem.*, **55**, 3398 (2012).
[24] Q. Wu, C. Fan, T. Chen, C. Liu, W. Mei, S. Chen, B. Wang, Y. Chen, W. Zheng. *Eur. J. Med. Chem.*, **63**, 57 (2013).
[25] L. He, S.Y. Liao, C.P. Tan, R.R. Ye, Y.W. Xu, M. Zhao, L.N. Ji, Z.W. Mao. *Chemistry*, **19**, 12152 (2013).
[26] A.M. Traynor, J.W. Lee, G.K. Bayer, J.M. Tate, S.P. Thomas, M. Mazurczak, D.L. Graham, J.M. Kolesar, J.H. Schiller. *Invest New Drugs*, **28**, 91 (2010).
[27] A.E. Stacy, D. Palanimuthu, P.V. Bernhardt, D.S. Kalinowski, P.J. Jansson, D.R. Richardson. *J. Med. Chem.*, **59**, 8601 (2016).
[28] D.J. Bauer. *Br. Med. Bull.*, **41**, 309 (1985).
[29] M.D. Hall, N.K. Salam, J.L. Hellawell, H.M. Fales, C.B. Kensler, J.A. Ludwig, G. Szakács, D.E. Hibbs, M.M. Gottesman. *J. Med. Chem.*, **52**, 3191 (2009).

[30] P.K. Yaman, B. Şen, C.S. Karagöz, E. Subaşı. *J. Organomet. Chem.*, **832**, 27 (2017).
[31] J. Haribabu, M.M. Tamizh, C. Balachandran, Y. Arun, N.S.P. Bhuvanesh, A. Endo, R. Karvembu. *New J. Chem.*, **42**, 10818 (2018).
[32] A. Gatti, A. Habtemariam, I.R. Canelon, J.I. Song, B. Heer, G.J. Clarkson, D. Rogolino, P.J. Sadler, M. Carcelli. *Organometallics*, **37**, 891 (2018).
[33] B. Dumat, E.F. Paul, P. Fornarelli, N. Saettel, G. Metgé, C.F. Debuisschert, F. Charra, F.M. Betzer, M.P.T. Fichou. *Org. Biomol. Chem.*, **14**, 358 (2016).
[34] Z. Wu, X. Fu, Y. Wang. *Sens. Actuators B*, **245**, 406 (2017).
[35] M.Q. Wang, L.X. Gao, Y.F. Yang, X.N. Xiong, Z.Y. Zheng, S. Li, Y. Wu, L.L. Ma. *Tetrahedron Lett.*, **57**, 504 (2016).
[36] A.K. Das, H. Ihmels, S. Kölsch. *Photochem. Photobiol. Sci.*, **18**, 1373 (2019).
[37] R. Chennoufi, H. Bougherara, N.G. Eilstein, B. Dumat, E. Henry, F. Subra, S. Bury Moné, F.M. Betzer, P. Tauc, M.P.T. Fichou, E. Deprez. *Sci. Rep.*, **6**, 21458 (2016).
[38] R. Mendoza-Merono, L. Menendez-Taboada, S. Garcia-Granda. *Acta Cryst.*, **68**, 2402 (2012).
[39] R.F. Brissos, P. Clavero, A. Gallen, A. Grabulosa, L.A. Barrios, A.B. Caballero, L. Korrodi-Gregorio, R.P. Tomas, G. Muller, V.S. Cerrato, P. Gamez. *Inorg. Chem.*, **57**, 14786 (2018).
[40] S.B. Jensen, S.J. Rodger, M.D. Spicer. *J. Organomet. Chem.*, **556**, 151 (1998).
[41] O.V. Reichmann, S.A. Rice, C.A. Thomas, P.J. Doty. *J. Am. Chem. Soc.*, **76**, 3047 (1954).
[42] R. Konakanchi, R. Mallela, R. Guda, L.R. Kotha. *Res. Chem. Intermed.*, **44**, 1 (2017).
[43] S. Sathiyaraj, R.J. Butcher, C.H. Jayabalakrishnan. *J. Mol. Struct.*, **1030**, 95 (2012).
[44] K.N. Kumar, G. Venkatachalam, R. Ramesh, Y. Liu. *Polyhedron*, **27**, 157 (2008).
[45] K. Jeyalakshmi, J. Haribabu, N.S.P. Bhuvanesh, R. Karvembu. *Dalton Trans.*, **45**, 12518 (2016).
[46] S. Swaminathan, J. Haribabu, N.K. Kalagatur, R. Konakanchi, N. Balakrishnan, N.S.P. Bhuvanesh, R. Karvembu. *ACS Omega*, **4**, 6245 (2019).
[47] R.N. Prabhu, R. Ramesh. *RSC Adv.*, **2**, 4515 (2012).
[48] M. Kalidasan, R. Nagarajaprakash, S. Forbes, Y. Mozharivskyj, K.M. Rao. *Z Anorg. Allg. Chem.*, **641**, 715 (2015).
[49] J. Haribabu, D.S. Ranade, N.S.P. Bhuvanesh, P.P. Kulkarni, R. Karvembu. *ChemistrySelect*, **2**, 11638 (2017).
[50] Y. Zhang, W. Huo, H.-Y. Zhang, J. Zhao. *RSC Adv.*, **7**, 47261 (2017).
[51] Q.L. Zhang, J.G. Liu, H. Chao, G.Q. Xue, L.N. Ji. *J. Inorg. Biochem.*, **83**, 49 (2001).
[52] M. Muralisankar, S. Sujith, N.S.P. Bhuvanesh, A. Sreekanth. *Polyhedron*, **118**, 103 (2016).
[53] M. Muralisankar, J. Haribabu, N.S.P. Bhuvanesh, R. Karvembu, A. Sreekanth. *Inorg. Chim. Acta*, **449**, 82 (2016).
[54] M. Muralisankar, R. Dheepika, J. Haribabu, C. Balachandran, S. Aoki, N.S.P. Bhuvanesh, S. Nagarajan. *ACS Omega*, **4**, 11712 (2019).
[55] J. Haribabu, K. Jeyalakshmi, Y. Arun, N.S.P. Bhuvanesh, P.T. Perumal, R. Karvembu. *RSC Adv.*, **5**, 46031 (2015).
[56] F.A. Beckford, G. Leblanc, J. Thessing, M. Shaloski, Jr., B.J. Frost, L. Li, N.P. Seeram. *Inorg. Chem. Commun.*, **12**, 1094(2009).
[57] E. Subasi, E.B. Atalay, D. Erdogan, B. Sen, B. Pakyapan, H.A. Kayali. *Mater. Sci. Eng. C Mater. Biol. Appl.*, **106**, 110152 (2020).
[58] M. Muralisankar, N.S.P. Bhuvanesh, A. Sreekanth. *New J. Chem.*, **40**, 2661(2016).
[59] B. Demoro, R.F.M. de Almeida, F. Marques, C.P. Matos, L. Otero, J.C. Pessoa, I. Santos, A. Rodríguez, V. Moreno, J. Lorenzo, D. Gambino, A.I. Tomaz. *Dalton Trans.*, **42**, 7131 (2013).
[60] P. Anitha, N. Chitrapriya, Y.J. Jang, P. Viswanathamurthi. *J. Photochem. Photobiol. B, Biol.*, **129**, 17 (2013).